Super-Resolution Imaging of Clickable Graphene Nanoribbons Decorated with Fluorescent Dyes

Dharati Joshi,[†,#] Meghan Hauser,[†,#] Gregory Veber,[†] Alexandra Berl,[†] Ke Xu,[†,‡,*] and Felix R. Fischer[†,§,¶,*]

[†]Department of Chemistry, University of California, Berkeley, CA 94720, USA.

[‡]Division of Molecular Biophysics and Integrated Bioimaging, Lawrence Berkeley National Laboratory, Berkeley, CA 94720, USA.

[§]Materials Sciences Division, Lawrence Berkeley National Laboratory, Berkeley, CA 94720, USA.

[¶]Kavli Energy NanoSciences Institute at the University of California Berkeley and the Lawrence Berkeley National Laboratory, Berkeley, California 94720, USA.

ABSTRACT: The functional integration of atomically-defined graphene nanoribbons (GNRs) into single ribbon electronic device architectures has been limited by access to non-destructive high-resolution imaging techniques that are both compatible with common supports like Si or Si/SiO_2 wafers and capable of resolving individual ribbons in dilute samples. Conventional techniques like scanning probe (AFM, STM) or electron microscopy (SEM, TEM) have been restricted by requisite sample preparation techniques that are incompatible with lithographic device fabrication. Here we report the design and synthesis of ultra-long (~10 μm) cove-type GNRs (cGNRs) featuring azide groups along the edges that can serve as a universal handle for late-stage functionalization with terminal alkynes. Copper catalyzed click-chemistry with Cy5 fluorescent dyes gives rise to cGNRs decorated along the edges with fluorescent tags detectable by optical microscopy. The structures of individual dye-functionalized cGNRs spin-coated from dilute solution onto transparent and opaque insulating substrates were resolved using diffraction-limited fluorescence microscopy and super-resolution microscopy (SRM) imaging techniques. Analysis of SRM images reveals an apparent width of cGNRs ranging between 40–50 nm and lengths in excess of 10 μm, the longest GNRs imaged to date. Isolated cGNRs can even be distinguished from bundles and larger aggregates as long as the center-to-center distance is greater than the apparent width.

INTRODUCTION

While narrow graphene nanoribbons (GNRs) share many of the unusual electronic properties of two-dimensional graphene, the lateral quantum confinement imposed by their finite width (< 2 nm) opens a sizable electronic band gap, elevating GNRs to a privileged position as a functional material for high-performance electronic device applications[1]. The intrinsic band gap of GNRs is tunable and is intimately linked to the width[2-5] and crystallographic symmetry of the ribbon[2-3, 6]. Any rational approach to tailoring the band structure of GNRs requires atomically-precise control over critical structural parameters such as width, length, and symmetry. As traditional top-down patterning techniques[7-11] lack the level of control required for precise bandgap engineering, recent examples of deterministic bottom-up approaches rely on the covalent growth of GNRs from small molecule building blocks[12-17] in solution or on catalytic metal surfaces. While bottom-up synthesized GNRs grown on a catalytically active metal surface can be imaged with atomically-resolved scanning probe microscopy (SPM), an imaging technique capable of resolving the detailed atomic and electronic structure of individual, immobilized GNRs, these advanced tools are not scalable to bulk processing and suffer from significant drawbacks (e.g. requirement of a metallic substrate) that hamper the integration of GNRs into single-ribbon electronic devices[18-19]. Solution-based approaches relying on either *Diels-Alder* or transition-metal catalyzed *Yamamoto* polymerizations followed by oxidative cyclodehydrogenation reactions have yielded bulk samples of cove- and chevron-type GNRs, yet critical challenges remain toward the incorporation of solution-synthesized GNRs into device architectures such as field effect transistors (FETs)[20]. The solution-processing of GNR dispersions, for example, is limited by the inherent insolubility and the tendency of GNRs to aggregate into bundles driven by non-covalent stacking interactions along the extended π-conjugated backbone[21]. While flakes of single-layer graphene can be readily visualized on SiO_2 and transparent substrates by optical microscopy[22-23], the spatial localization of narrow solution-processed GNRs on insulating substrates required for aligning lithographic masks used in device fabrication remains a daunting challenge. Traditional imaging techniques like atomic force microscopy (AFM)[24-25], transmission electron microscopy (TEM)[26], scanning electron microscopy (SEM)[25-26], and scanning tunneling microscopy (STM)[12-13, 24-25] are either restricted to atomically flat substrates (e.g., mica, graphite), require the sample to be suspended on a fragile, atomically thin support, or are restricted to conductive surfaces incompatible with electronic device architectures. While the lateral resolution of traditional optical microscopy is limited by the diffraction of light (~300 nm), recent advancements in super-resolution microscopy (SRM) have enabled sub-diffraction imaging of nanoscale structures in biological specimens[27-28] and even some selected functional materials[29-33].

We herein report the late-stage covalent functionalization of solution-synthesized cove-type GNRs (cGNRs) with fluorescent dyes and their optical visualization on insulating substrates using SRM. Our synthetic modification of cGNRs introduces an azide functional group in the solubilizing side chains of cGNRs that can both be conjugated to a large variety of commercial fluorescent dyes, and also

represents a universal linker for the covalent functionalization of GNRs through click-chemistry. A direct correlation of conventional diffraction-limited optical microscopy and SRM of Cy5-functionalized cGNRs reveals that isolated individual ribbons and even aggregates and bundles of cGNRs can be resolved down to the apparent width of ~40–50 nm.

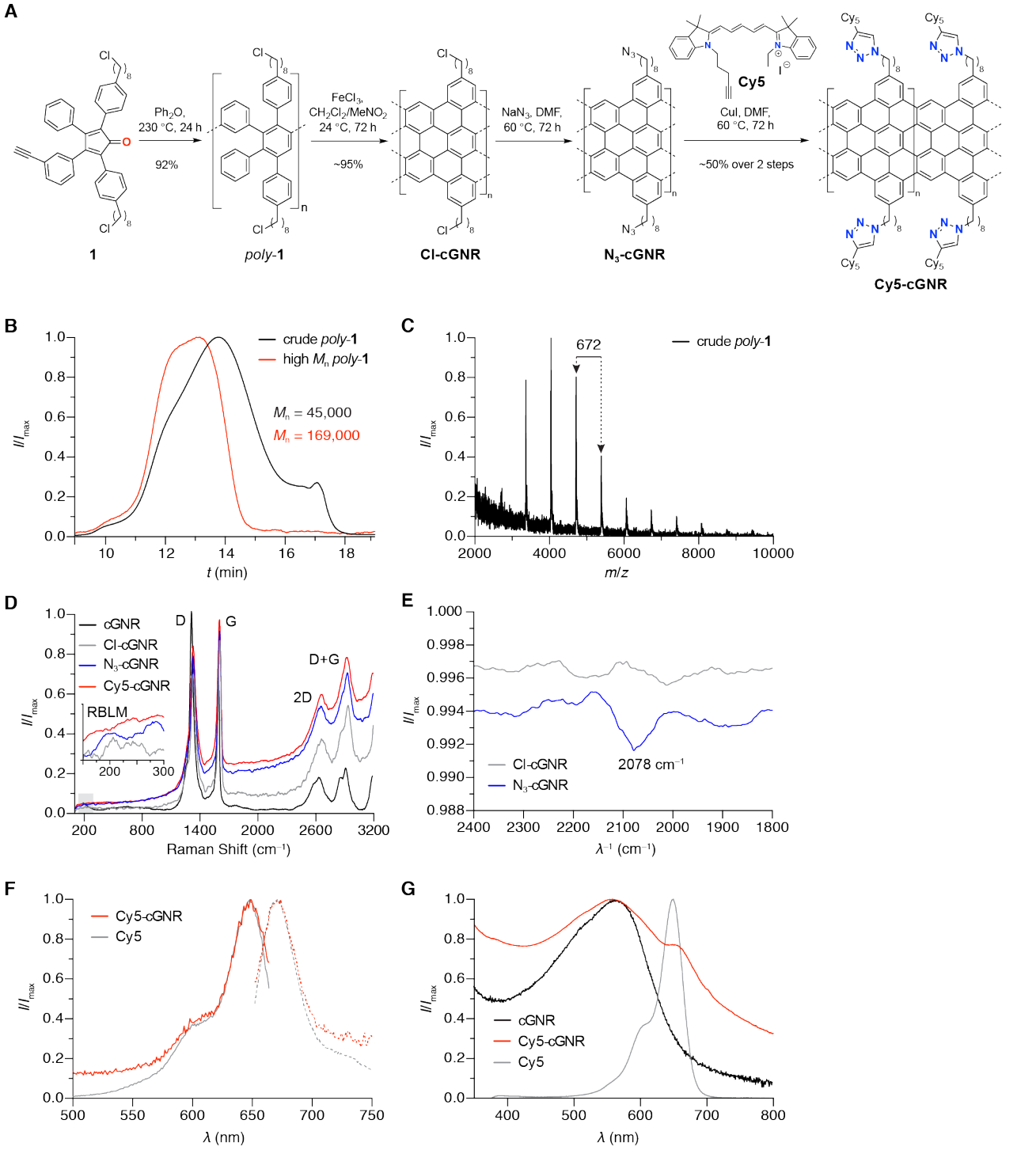

Figure 1. Synthesis and characterization of dye-functionalized Cy5-cGNRs. (A) Schematic representation of the synthesis of clickable **N$_3$-cGNRs** and their functionalization with a Cy5 dye bearing a terminal alkyne. (B) Size exclusion chromatography (SEC) trace of crude *poly*-**1** (black) and the high molecular weight fraction (red) isolated by preparative SEC. (C) MALDI mass spectrum of crude *poly*-**1** showing the characteristic family of molecular ions. The spacing corresponds to the mass of the polymer repeat unit. (D) Raman spectrum (λ_E = 514 nm) of bulk samples of unsubstituted **cGNRs**, **Cl-cGNRs**, **N$_3$-cGNRs**, and **Cy5-cGNRs**. Inset shows a magnification of the spectral region associated with the RBLM. (E) IR spectrum of **Cl-cGNRs** and **N$_3$-cGNRs** showing the characteristic peak associated with the azide stretching mode. (F) Fluorescence excitation (solid lines) and emission (dotted lines) spectra of free Cy5 and dye-functionalized **Cy5-cGNRs**. (G) UV-Vis absorption spectra of unsubstituted **cGNRs**, free Cy5, and dye-functionalized **Cy5-cGNRs**.

Comparison of SRM images with AFM of a carbon nanotube reference reveals that our super-resolution techniques represent a versatile, non-destructive tool to localize individual ribbons and even complex graphene nanostructures on insulating substrates suitable for electronic device fabrication.

RESULTS AND DISCUSSION

The solution-based bottom-up synthesis of fluorescent dye-functionalized cGNRs (**Cy5-cGNR**) is depicted in Figure 1A. Since neither the dye (Cy5) nor the azide group required for the click-chemistry is compatible with the harsh reaction conditions associated with the oxidative cyclodehydrogenation of the GNR precursor polymers, we designed a synthetic route around a late-stage functional group interconversion: a nucleophilic substitution of an alkyl chloride with an azide on the fully graphitized GNR. *Diels-Alder* polymerization and decarbonylation of cyclopentadienone **1** featuring two (8-chlorooctyl)benzene substituents yielded the polyphenylene intermediate *poly*-**1** in 92% yield. The molecular weight dispersity, $Đ_M$, of *poly*-**1** derived from size exclusion chromatography (SEC, calibrated to polystyrene standards) ranges from 2.5 to 3.9 with a number average molecular weight M_n of 45 kg mol^{-1} (Figure 1B). Preparative SEC yielded a high molecular weight fraction of *poly*-**1** with $Đ_M$ = 1.7 and a M_n of 169 kg mol^{-1} that was carried on through the rest of the synthesis. MALDI mass spectrometry (Figure 1C) shows the characteristic family of molecular ions separated by the mass of the decarbonylated monomer **1** (ΔM = 672 g mol^{-1}). Oxidative cyclodehydrogenation of *poly*-**1** yields structurally homogeneous cGNRs (**Cl-cGNR**) featuring solubilizing 8-chlorooctyl side chains along the protrusions of the cove-edges. Raman spectroscopy (λ_E = 532 nm) shows the characteristic signatures for the radial breathing like mode (RBLM)[16,34] (232 cm^{-1}; FWHM = 83 cm^{-1}), the D (1334 cm^{-1}; FWHM = 56 cm^{-1}) and G (1607 cm^{-1}; FWHM = 26 cm^{-1}) peaks with a ratio of $I_{D/G}$ = 0.76 along with higher order 2D and D+G peaks (Figure 1D). Nucleophilic substitution of the primary chlorides in the solubilizing side chains of **Cl-cGNR** with sodium azide gave the clickable cGNRs (**N_3-cGNR**). A comparison of the infrared spectra of **Cl-cGNR** and **N_3-cGNR** (Figure 1E) reveals the appearance of a characteristic absorption peak (λ^{-1} = 2078 cm^{-1}) assigned to the azide linear stretching mode[35]. The Raman spectrum of **N_3-cGNR** shows no significant change in the RBLM, D and G peak position/ratio, consistent with the selective attack of the azide on the ancillary alkyl chloride side chain rather than a functionalization of the conjugated backbone of the cGNRs. Copper-catalyzed *Huisgen* 1,3-dipolar cycloaddition between **N_3-cGNRs** and a Cy5 dye bearing a terminal alkyne gave the dye-functionalized **Cy5-cGNRs** in ~50% yield over two steps (determined by elemental analysis, Supporting Information Figure S1). Fluorescence and UV-Vis spectroscopy show the successful integration of the dye with the cGNRs (Figure 1F,G). The fluorescence excitation and emission spectra of **Cy5-cGNRs** are almost indistinguishable from the spectra of free Cy5, indicating that the alkyl spacers between the dye and the extended π-system of the cGNR effectively prevent quenching of excited states. The excitation (emission) maxima are found at 649 nm (674 nm) and 648 nm (671 nm) for the **Cy5-GNRs** and Cy5, respectively. While free Cy5 shows a maximum UV-Vis absorption at λ_{max} = 650 nm the corresponding transition in the dye-functionalized **Cy5-GNRs** is slightly red-shifted and appears as a shoulder around λ = 663 nm.

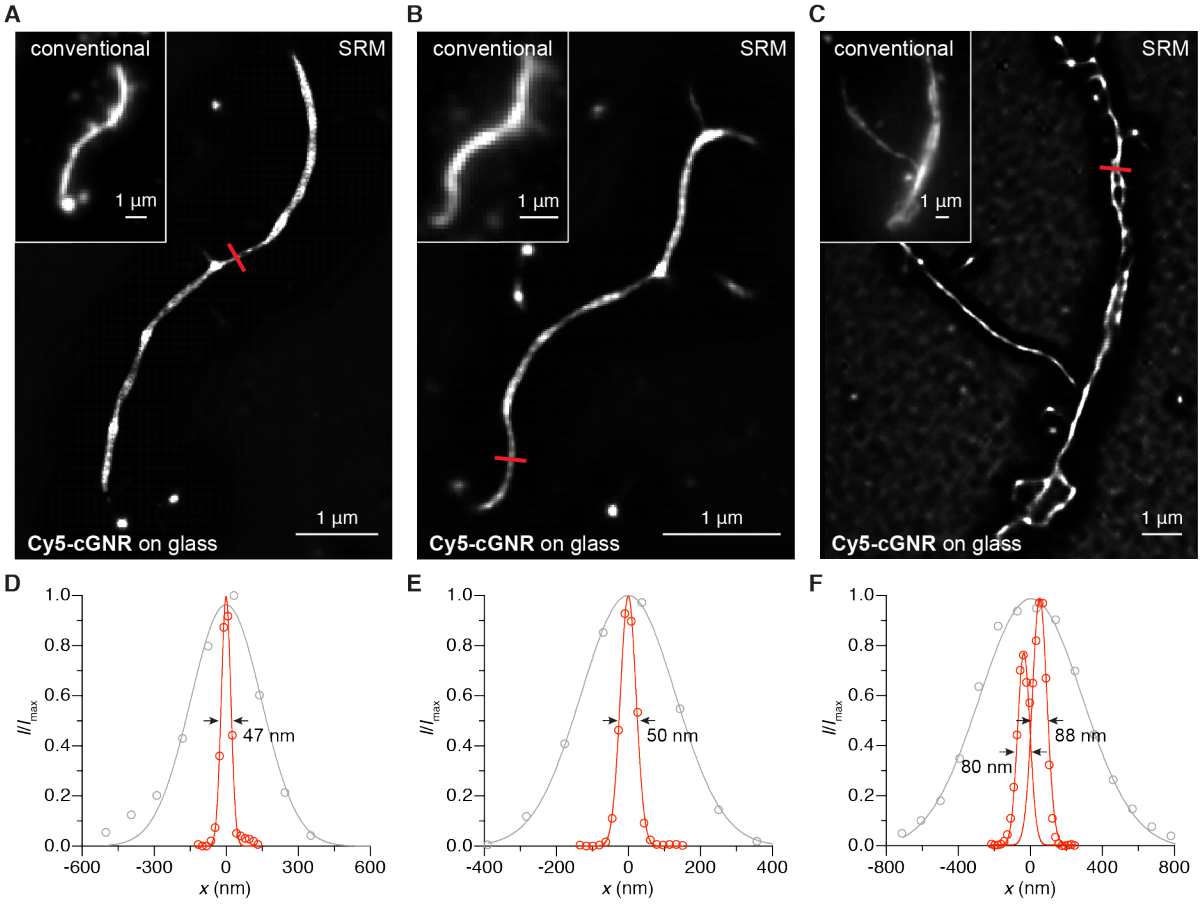

Figure 2 Comparison between conventional fluorescence and super-resolution microscopy of dye-functionalized **Cy5-cGNRs.** (A–C) SRM (SRRF) fluorescence images of samples of **Cy5-cGNRs** on silanized glass coverslips. Figure insets show conventional diffraction-limited microscopy of the same area of the sample. (D–F) Fluorescence intensity cross-section profiles at positions highlighted (red lines) in A–C in conventional diffraction-limited fluorescence microscopy (gray) and SRM (SRRF) images (red) (circles: experimental data, lines: Gaussian fits). The SRM data in (F) is fitted by two Gaussian peaks with a 98 nm peak-to-peak distance.

Samples of dye-functionalized GNRs for fluorescence imaging were prepared by spin-coating dilute suspensions (0.1 mg mL^{-1}) of **Cy5-cGNRs** in acetone first onto silanized glass coverslips. Raman mapping of the G peak intensity reveals a homogenous coverage of the surface with **Cy5-cGNRs** with only minimal aggregation into larger bundles (Supporting Information Figure S2). Conventional, diffraction-limited fluorescence microscopy (laser λ_{Ex} = 647 nm; 2 mW cm^{-2}) of **Cy5-cGNRs** on glass coverslips reveals isolated fluorescent strings and larger bundles with typical apparent lengths ranging between 5–15 µm (Figure 2A–C insets). Fluorescence intensity cross-section profiles of individual **Cy5-cGNRs** show apparent full width at half maximum (FWHM) of ~300 nm (gray circles and lines in Figure 2D–E), well in agreement with the expected diffraction limit given the emission wavelength of Cy5 (λ_{Em} = 671 nm). While conventional fluorescence microscopy of **Cy5-cGNRs** clearly reveals the position of dye-functionalized cGNRs even on an insulating non-planar substrate, the resolution is insufficient to unambiguously distinguish between single **Cy5-cGNRs** and larger bundles.

To increase the lateral resolution and to identify the number and the arrangement of cGNRs in a specific sample, we imaged the same structures using SRM. The sample slide was immersed in an imaging buffer containing 2-aminoethanethiol to assist the photoswitching/blinking of Cy5 dyes, and the laser power was increased to 2 kW cm^{-2}. Under these routine STORM (stochastic optical reconstruction microscopy) SRM conditions[36], the majority of the Cy5-dyes were expected to reside in a non-fluorescent dark state, and only the small number of emitting molecules distributed across a frame contribute to the single-molecule localization. Unexpectedly, we found that even at the highest concentration of thiol quencher (100 mM), the inherent fluorescence of the Cy5 dyes lining the edges of **Cy5-cGNRs** could never be entirely switched to the dark state. As a result, we observed overlapping emissions from closely localized dye molecules in imaging frames (see Supporting Information Figure S3 for representative frames) that prevented us from performing single-molecule localization analysis required for STORM. This effect is likely due to a combination of the unusually high density of dyes along the edges of the cGNR (~1–2 Cy5 dyes nm^{-1}) and the hydrophobic local environment of the cGNR that limits the local concentration of thiol quencher.

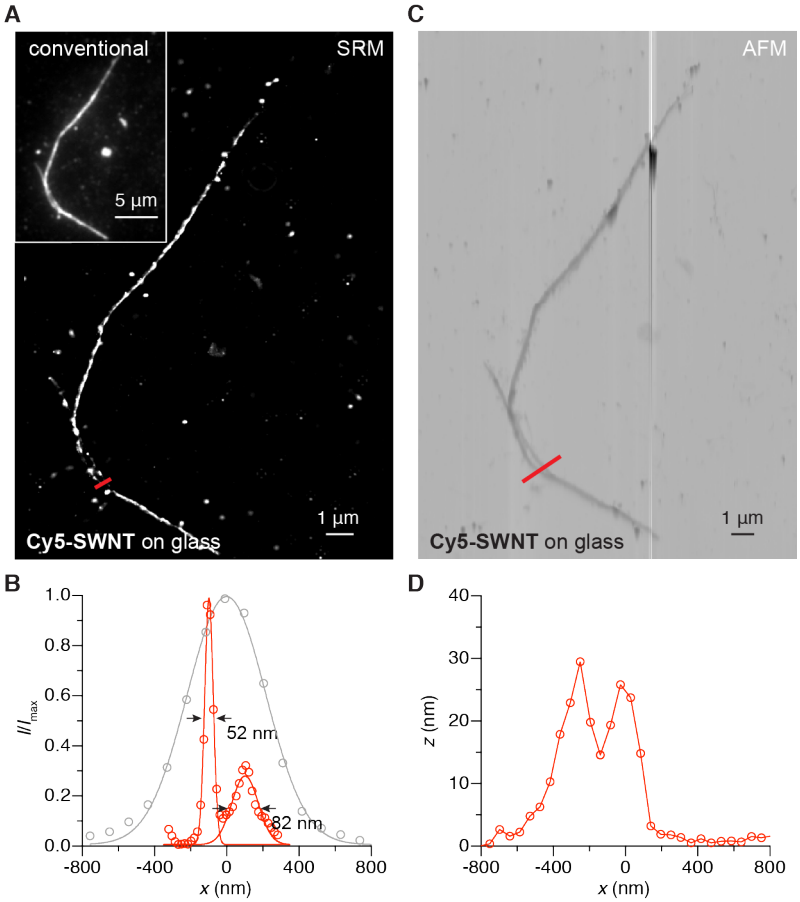

Figure 3 Conventional fluorescence, super-resolution, and atomic force microscopy of dye-functionalized **Cy5-SWNTs**. (A) SRM (SRRF) fluorescence image of **Cy5-SWNTs** on a glass coverslip. Figure inset shows conventional diffraction-limited microscopy of the same area of the sample. (B) Fluorescence intensity cross-section profiles at positions highlighted (red lines) in (A) in the conventional diffraction-limited fluorescence microscopy (gray) and SRM (SRRF) (red) images (circles: experimental data, lines: Gaussian fits). (C) AFM image of the same area of the sample depicted in (A). (D) AFM height profile of **Cy5-SWNTs** at the position highlighted (red line) in (C).

While we were unable to attain efficient single-molecule switching required for STORM, we observed significant temporal fluorescence intensity fluctuations along the length of **Cy5-cGNRs** (Supporting Information Figure S3). This temporal variation of the fluorescence intensity of images collected in different frames allowed us to apply super-resolution optical fluctuation imaging (SOFI)[37] and super-resolution radial fluctuation (SRRF)[38] analysis methods. Figures 2A,B show SRRF images of the two distinct **Cy5-cGNRs** corresponding to the diffraction-limited images depicted in the figure insets. Intensity cross-section profiles show an apparent FWHM of 47–50 nm for both dye-functionalized cGNRs. Assuming the backbone of the cGNRs adsorbs planar and parallel to the surface, the theoretically predicted width of **Cy5-cGNRs** is expected to range between 7–10 nm. The uniform apparent width of ~50 nm observed across numerous different **Cy5-cGNRs** samples (see Supporting Information Figure S4 for additional images) suggests that single isolated **Cy5-cGNRs** can be resolved with an apparent width close to the reported theoretical resolution limit of SRRF[38]. An analysis of multiple images of dye-functionalized cGNRs suggests that it is not unusual for single ribbons to reach lengths of 6–10 µm corresponding to 8,000–12,000 linearly fused monomer units, the longest bottom-up synthesized GNRs reported to date[16, 25, 39].

SRRF imaging of dye-functionalized **Cy5-cGNRs** not only represents a ~10-fold improvement over the resolution of diffraction-limited fluorescence microscopy images (Figure 2A–C insets) but further provides a reliable tool to analyze structures comprised of entangled cGNR bundles and potentially even more complex functional arrays. Figure 2C shows both a conventional fluorescence image and a SRRF image of a **Cy5-cGNR** bundle comprised of entangled cGNRs. The fluorescence intensity cross-section profile for a region of the diffraction-limited image shows a single unresolved broad peak with a FWHM of 670 nm. In contrast, the corresponding SRRF image reveals two parallel cGNRs. The intensity cross-section profile shows two well-separated peaks at 98 nm center-to-center distance with FWHMs of 80 nm and 88 nm respectively. This example demonstrates that SRRF imaging of dye-functionalized GNRs can resolve structural details well below the resolution limit imposed by the diffraction of light.

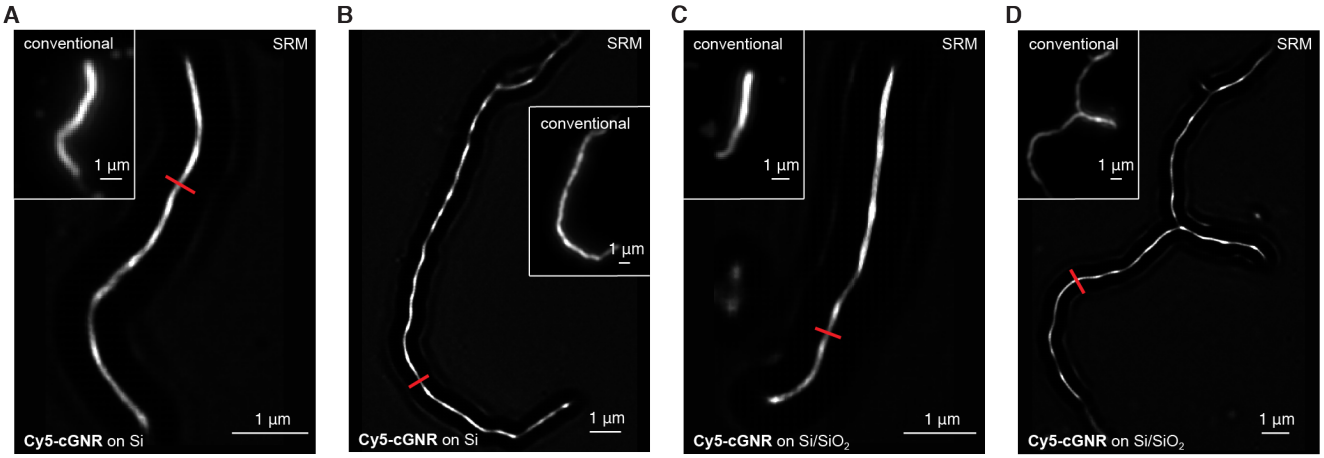

Figure 4. Comparison between conventional fluorescence and super-resolution microscopy of dye-functionalized Cy5-cGNRs on Si and Si/SiO_2 wafers. (A–B) SRM (SRRF) fluorescence images of samples of Cy5-cGNRs on silanized Si wafers. Figure insets show the conventional diffraction-limited microscopy of the same area of the sample. (C–D) SRM (SRRF) fluorescence images of samples of Cy5-cGNRs on silanized Si/SiO_2 wafers (SiO_2 thickness ~ 300 nm). Figure insets show the conventional diffraction-limited microscopy of the same area of the sample.

In an effort to corroborate the apparent width of **Cy5-cGNRs** derived from SRRF analysis to the real dimensions of the ribbon we selected single wall carbon nanotubes (SWNTs) as a reference standard that could be independently verified by atomic force microscopy (AFM) (we were unable to resolve cGNRs on glass directly as the surface roughness of glass coverslips is greater than the apparent height of individual graphene nanoribbons). Covalent functionalization of SWNTs with (2-azidoethoxy)benzene followed by copper-catalyzed *Huisgen* 1,3-dipolar cycloaddition with *N*-pentynyl-Cy5 gave the corresponding dye-functionalized SWNTs (**Cy5-SWNT**, Supporting Information Figure S5). Figure 3A shows conventional fluorescence and SRRF microscopy images of **Cy5-SWNTs** spin-cast from dilute solution onto glass coverslips. The fluorescence intensity cross-section profile reveals an apparent width of 52–82 nm for individual carbon nanotubes. Analogous to our studies on **Cy5-cGNRs**, nanotubes within larger aggregates or bundles can be resolved by SRRF when separated by distances greater than the apparent width of a **Cy5-SWNT** (Figure 3A,B). A correlation of **Cy5-SWNT** structures imaged by SRM with AFM height profiles recorded at the same position (Figure 3C,D) reveals that the ~50 nm wide features resolved in our SRRF SRM images indeed correspond to individual SWNTs.

While non-destructive SRM imaging of dye-functionalized cGNRs and SWNTs on glass coverslips serves as a proof of concept, the greater challenge lies in transferring this tool to more relevant substrates like bare Si or Si/SiO_2 wafers traditionally used in electronic device fabrication. SRM imaging on these opaque substrates was achieved by inverting the sample geometry and imaging through an opposing coverslip. Representative images of linear strings and small bundles of **Cy5-cGNRs** spin-coated from solution onto silanized Si and Si/SiO_2 wafers are depicted in Figure 4A,B and Figure 4c,d, respectively. Fluorescence intensity cross-section profiles of SRRF images on both bare Si and SiO_2 show a FWHM of 60–68 nm (Supporting Information Figure S6) reminiscent of the apparent width of **Cy5-cGNRs** on glass slides. This work demonstrates that SRM (SRRF) of dye-functionalized cGNRs can be used as a non-destructive, high-throughput, high-resolution imaging tool to localize individual isolated ribbons in the very dilute samples required for the targeted deposition of lithographic contacts in the fabrication of experimental electronic device architectures.

CONCLUSION

In conclusion, we have developed a solution-based synthesis of a new class of cGNRs functionalized with reactive azide groups along the edges that can undergo Cu-catalyzed click-reactions with a wide variety of functional groups and molecules bearing a terminal alkyne. We have demonstrated that conjugation of these clickable cGNRs with fluorescent dyes derived from Cy5 allows the imaging of dilute dispersions of cGNRs spin-coated onto glass, Si, or Si/SiO_2 substrates using not only conventional fluorescence but also super-resolution microscopy (SRM). While the apparent width of individual ribbons imaged by SRM is well below the diffraction limit of light and allows the unambiguous distinction between isolated ribbons and larger bundles on the surface, a statistical analysis of the length of **Cy5-cGNRs** reveals that the exceptionally efficient *Diels-Alder* polymerization of cGNR monomers can give rise to graphene nanoribbons ranging in length from 6–10 μm. This work not only describes the development of a highly versatile and modular material based on azide-functionalized GNRs, but also demonstrates that one of the critical challenges in the exploration and exploitation of the exotic properties of GNRs in electronic devices, the non-destructive imaging of dilute samples on opaque dielectric substrates, can be accomplished using super-resolution fluorescence imaging techniques derived from cell biology.

EXPERIMENTAL SECTION

Materials and General Methods. Unless otherwise stated, all manipulations of air- and/or moisture-sensitive compounds were carried out in oven-dried glassware, under an atmosphere of N_2. All solvents and reagents were purchased from Alfa Aesar, Spectrum Chemicals, Acros Organics, TCI America, and Sigma-Aldrich and were used as received unless otherwise noted. Organic solvents were dried by passing through a column of alumina and were degassed by vigorous bubbling of N_2 or Ar through the solvent for 20 min. Flash column chromatography was performed on SiliCycle silica gel (particle size 40–63 μm). Thin layer chromatography was performed using SiliCycle silica gel 60 Å F-254 precoated plates (0.25 mm thick) and visualized by UV absorption. All ^1H and ^{13}C NMR spectra were recorded on Bruker AVB-400, AVQ-400, and AV-600 MHz spectrometers, and are referenced to residual solvent peaks ($CDCl_3$ ^1H NMR = 7.26 ppm, ^{13}C NMR = 77.16 ppm; CD_2Cl_2 ^1H NMR = 5.32 ppm, ^{13}C NMR = 54.00 ppm). ESI mass spectrometry was performed on a Finnigan LTQFT (Thermo) spectrometer in positive ionization mode. MALDI mass spectrometry was performed

on a Voyager-DE PRO (Applied Biosystems Voyager System 6322) in positive mode using a matrix of dithranol. Elemental analysis (CHN) was performed on a Perkin Elmer 2400 Series II combustion analyzer. Gel permeation chromatography (GPC) was performed on a LC/MS Agilent 1260 Infinity set up with one guard and two Agilent Polypore 300 x 7.5 mm columns at 35 °C. All GPC analyses were performed on a 0.2 mg/mL solution of polymer in chloroform. An injection volume of 25 μL and a flow rate of 1 mL min^{-1} were used. Calibration was based on narrow polydispersity polystyrene standards ranging from M_w = 100 to 4,068,981 g mol^{-1}. Infrared spectroscopy was performed on a Bruker ALPHA ATR-FTIR. Raman spectroscopy was performed on a Renishaw inVia spectrometer with 514 nm excitation laser. Raman mapping was performed on a Horiba Jobin Yvon LabRAM ARAMIS confocal Raman microscope with 532 nm excitation wavelength.

Preparation of poly-1 A 10 mL Schlenk flask was charged under N_2 with **1** (45.3 mg, 0.0645 mmol) in Ph_2O (0.042 mL). The reaction mixture was degassed by three freeze-pump-thaw cycles. The reaction mixture was stirred at 230 °C for 24 h. The reaction mixture was diluted with MeOH and the precipitate was collected via centrifugation. The solid residue was dissolved in THF, triturated with MeOH, and collected via centrifugation to yield *poly*-**1** (39.9 mg, 92%) as a colorless solid. The crude polymers were fractionated by preparative GPC. ^1H NMR (400 MHz, CH_2Cl_2, 22 °C) δ = 7.18–6.19 (m, 18H), 3.52 (t, *J* = 6.1 Hz, 4H), 2.68–2.30 (m, 4H), 1.81–1.68 (m, 4H), 1.64–1.08 (m, 20H) ppm.

Preparation of Cl-cGNR A 500 mL Schlenk flask was charged under N_2 with *poly-**1*** (10.5 mg) in CH_2Cl_2 (80 mL). A suspension of $FeCl_3$ (212 mg, 1.31 mmol, 7 equiv for each hydrogen to be removed) in $MeNO_2$ (4 mL) was added. The reaction mixture was stirred at 24 °C for 72 h under a continuous stream of N_2. The reaction mixture was quenched with MeOH and filtered. Washing the precipitate with MeOH (500 mL), 1M HCl (300 mL), H_2O (1000 mL), and THF (500 mL), yielded **Cl-cGNR** as a black powder (10.3 mg, 95%). Raman (powder): 1334, 1607, 2654, 2937 cm^{-1}.

Preparation of N_3-cGNR A 25 mL vial was charged with **Cl-cGNR** (10.6 mg) in DMF (20 mL). The reaction mixture was sonicated for 1.5 h under N_2. NaN_3 (500 mg, 7.69 mmol) was added and the reaction mixture sonicated for 30 min. The reaction mixture was stirred at 60 °C for 18 h under N_2. The reaction mixture was sonicated for 4 h and stirred at 60 °C for an additional 18 h under N_2. The reaction mixture was sonicated for 1 h and filtered. Washing the precipitate with H_2O (1000 mL) and THF (500 mL) yielded **N_3-cGNR** as a black powder (10.8 mg). Raman (powder): 1329, 1607, 2657, 2934 cm^{-1}.

Preparation of Cy5-cGNR A 25 mL vial was charged with **N_3-cGNR** (5.5 mg), *N*-pentynyl-Cy5 (21.1 mg, 0.0375 mmol), and CuI (60 mg, 0.315 mmol) in DMF (20 mL). The reaction mixture was sonicated for 2 h and stirred at 60 °C for 18 h under N_2. The reaction mixture was sonicated for 2 hours and stirred for an additional 18 h under N_2. The reaction mixture was sonicated for 2 h and filtered. The precipitate was washed with acetone (1000 mL), MeOH (1000 mL), H_2O (500 mL), DMF (300 mL), CH_2Cl_2 (300 mL) and THF (500 mL) until the filtrate was colorless/non-fluorescent to yielded **Cy5-cGNR** as a black powder (8.5 mg). Raman (powder): 1329, 1604, 2672, 2928 cm^{-1}; Anal. Calcd. for $(C_{108}H_{108}I_2N_{10})_n$: C, 72.07; H, 6.05; N, 7.78. Found: C, 43.81; H, 5.82; N, 3.63.

Sample Preparation and Imaging. Cy5-cGNRs were dispersed in acetone at 0.1 mg mL^{-1} by probe sonication for 30 min, and subsequently spin-coated at 5000 rpm onto glass coverslips and silicon wafers with and without a 300 nm thick thermal oxide layer functionalized with chlorotrimethylsilane (Alfa Aesar A13651). Cy5-SWNTs were dispersed at 0.1 mg mL^{-1} in deionized water by probe sonication for 30 min, and then spin-coated at 5000 rpm onto unfunctionalized glass coverslips. The samples were then mounted onto a glass side with a Tris-Cl imaging buffer (pH 7.5) containing 100 mM 2-aminoethanethiol, 5% glucose, 0.8 mg mL^{-1} glucose oxidase, and 40 μg mL^{-1} catalase. Epifluorescence microscopy and SRM imaging were performed on a homebuilt setup based on a Nikon Eclipse Ti-E inverted optical microscope using an oil-immersion objective (Nikon CFI Plan Apochromat λ 100 ×, numerical aperture = 1.45) with additional 1.5 × magnification on the microscope. Laser at 647 nm (MPB Communications) was coupled into an optical fiber after an acousto-optic tunable filter and then introduced into the sample through the back focal plane of the objective via a dichroic mirror (ZT640rdc, Chroma). Using a translation stage, the laser beam was shifted toward the edge of the objective so that emerging light reached the sample at an incidence angle close to the critical angle of the glass-water interface to achieve total internal reflection. Continuous illumination of 647 nm laser was used to excite fluorescence from Cy5 molecules. Emission was filtered by a long-pass (ET655lp, Chroma) and a band-pass (ET700/75m, Chroma) filter, and recorded with an EM-CCD (electron-multiplying charge-coupled device) camera (iXon Ultra 897, Andor) at 110 frames s^{-1} for a frame size of 256 × 256 pixels. Diffraction-limited images were first taken at typical illumination intensities of 2 mW cm^{-2}. SRM raw data were then taken at typical illumination intensities of 2 kW cm^{-2} for 20,000 frames. Super-resolution radial fluctuation (SRRF) analysis was performed using a published ImageJ plugin[38]. Algorithm was temporal radiality auto-cumulant order 2 (TRAC2), and optimized parameters were ring radius of 0.5, radiality magnification of 6, 6 axes in ring, with intensity weighting, and without renormalization. Approximately 4,000 frames were used to construct the final SRRF image.

ASSOCIATED CONTENT

Supporting Information

The Supporting Information is available free of charge on the ACS Publications website.

Elemental analysis (Figure S1)
Raman maps of **Cy5-cGNRs** on glass cover slips (Figure S2)
SRM images of **Cy5-cGNRs** (Figure S3–S4);
characterization of **Cy5-SWNTs** (Figure S5);
fluorescence intensity cross-section profiles (Figure S6)
synthetic procedures for **1**;
NMR spectra (Figure S7–S21)

AUTHOR INFORMATION

Corresponding Author

*xuk@berkeley.edu; ffischer@berkeley.edu

Author Contributions

#These authors contributed equally to this work.
All authors approved the final version of the manuscript.

ACKNOWLEDGMENT

Research supported by the U.S. Department of Energy (DOE), Office of Science, Basic Energy Sciences (BES), under award no. DE-SC0010409 (design, synthesis, and characterization of molecules and materials), and by STROBE, a National Science Foundation Science and Technology Center under Grant No. DMR 1548924 (SRM imaging). Berkeley NMR Facility is supported in part by NIH grant SRR023679A. D.J. acknowledges support through a National Science Foundation Graduate Research Fellowship under Grant # DGE-1106400.

REFERENCES

(1) Shen, H. L.; Shi, Y.; Wang, X. R. *Synthetic Metals* **2015**, *210*, 109-122.
(2) Barone, V.; Hod, O.; Scuseria, G. E. *Nano Lett.* **2006**, *6*, 2748-2754.
(3) Nakada, K.; Fujita, M.; Dresselhaus, G.; Dresselhaus, M. S. *Physical Review B* **1996**, *54*, 17954-17961.
(4) Son, Y. W.; Cohen, M. L.; Louie, S. G. *Physical Review Letters* **2006**, *97*, 216803.
(5) Yang, L.; Park, C. H.; Son, Y. W.; Cohen, M. L.; Louie, S. G. *Physical Review Letters* **2007**, *99*, 186801.
(6) Fujita, M.; Wakabayashi, K.; Nakada, K.; Kusakabe, K. *Journal of the Physical Society of Japan* **1996**, *65*, 1920-1923.
(7) Chen, Z. H.; Lin, Y. M.; Rooks, M. J.; Avouris, P. *Physica E* **2007**, *40*, 228-232.

(8) Datta, S. S.; Strachan, D. R.; Khamis, S. M.; Johnson, A. T. C. *Nano Lett.* **2008**, *8*, 1912-1915.
(9) Elias, A. L.; Botello-Mendez, A. R.; Meneses-Rodriguez, D.; Gonzalez, V. J.; Ramirez-Gonzalez, D.; Ci, L.; Munoz-Sandoval, E.; Ajayan, P. M.; Terrones, H.; Terrones, M. *Nano Lett.* **2010**, *10*, 366-372.
(10) Kosynkin, D. V.; Higginbotham, A. L.; Sinitskii, A.; Lomeda, J. R.; Dimiev, A.; Price, B. K.; Tour, J. M. *Nature* **2009**, *458*, 872-876.
(11) Wang, X. R.; Dai, H. J. *Nat. Chem.* **2010**, *2*, 661-665.
(12) Cai, J. M.; Ruffieux, P.; Jaafar, R.; Bieri, M.; Braun, T.; Blankenburg, S.; Muoth, M.; Seitsonen, A. P.; Saleh, M.; Feng, X. L.; Müllen, K.; Fasel, R. *Nature* **2010**, *466*, 470-473.
(13) Chen, Y. C.; de Oteyza, D. G.; Pedramrazi, Z.; Chen, C.; Fischer, F. R.; Crommie, M. F. *ACS Nano* **2013**, *7*, 6123-6128.
(14) Cloke, R. R.; Marangoni, T.; Nguyen, G. D.; Joshi, T.; Rizzo, D. J.; Bronner, C.; Cao, T.; Louie, S. G.; Crommie, M. F.; Fischer, F. R. *J. Am. Chem. Soc.* **2015**, *137*, 8872-8875.
(15) Durr, R. A.; Haberer, D.; Lee, Y. L.; Blackwell, R.; Kalayjian, A. M.; Marangoni, T.; Ihm, J.; Louie, S. G.; Fischer, F. R. *J. Am. Chem. Soc.* **2018**, *140*, 807-813.
(16) Narita, A.; Feng, X. L.; Hernandez, Y.; Jensen, S. A.; Bonn, M.; Yang, H. F.; Verzhbitskiy, I. A.; Casiraghi, C.; Hansen, M. R.; Koch, A. H. R.; Fytas, G.; Ivasenko, O.; Li, B.; Mali, K. S.; Balandina, T.; Mahesh, S.; De Feyter, S.; Müllen, K. *Nat. Chem.* **2014**, *6*, 126-132.
(17) Vo, T. H.; Shekhirev, M.; Lipatov, A.; Korlacki, R. A.; Sinitskii, A. *Faraday Discussions* **2014**, *173*, 105-113.
(18) Bennett, P. B.; Pedramrazi, Z.; Madani, A.; Chen, Y. C.; de Oteyza, D. G.; Chen, C.; Fischer, F. R.; Crommie, M. F.; Bokor, J. *Appl. Phys. Lett.* **2013**, *103*, 253114.
(19) Llinas, J. P.; Fairbrother, A.; Barin, G. B.; Shi, W.; Lee, K.; Wu, S.; Choi, B. Y.; Braganza, R.; Lear, J.; Kau, N.; Choi, W.; Chen, C.; Pedramrazi, Z.; Dumslaff, T.; Narita, A.; Feng, X. L.; Müllen, K.; Fischer, F.; Zettl, A.; Ruffieux, P.; Yablonovitch, E.; Crommie, M.; Fasel, R.; Bokor, J. *Nat. Comm.* **2017**, *8*, 633.
(20) Abbas, A. N.; Liu, G.; Narita, A.; Orosco, M.; Feng, X. L.; Müllen, K.; Zhou, C. W. *J. Am. Chem. Soc.* **2014**, *136*, 7555-7558.
(21) Shekhirev, M.; Vo, T. H.; Kunkel, D. A.; Lipatov, A.; Enders, A.; Sinitskii, A. *Rsc Advances* **2017**, *7*, 54491-54499.
(22) Blake, P.; Hill, E. W.; Castro Neto, A. H.; Novoselov, K. S.; Jiang, D.; Yang, R.; Booth, T. J.; Geim, A. K. *Appl. Phys. Lett.* **2007**, *91*, 063124.
(23) Li, W.; Moon, S.; Wojcik, M.; Xu, K. *Nano Lett.* **2016**, *16*, 5027-5031.
(24) Marangoni, T.; Haberer, D.; Rizzo, D. J.; Cloke, R. R.; Fischer, F. R. *Chemistry-a European Journal* **2016**, *22*, 13037-13040.
(25) Vo, T. H.; Shekhirev, M.; Kunkel, D. A.; Morton, M. D.; Berglund, E.; Kong, L. M.; Wilson, P. M.; Dowben, P. A.; Enders, A.; Sinitskii, A. *Nat. Comm.* **2014**, *5*, 8.
(26) Jiao, L. Y.; Wang, X. R.; Diankov, G.; Wang, H. L.; Dai, H. J. *Nat. Nanotechnol.* **2010**, *5*, 321-325.
(27) Huang, B.; Babcock, H.; Zhuang, X. *Cell* **2010**, *143*, 1047-1058.
(28) Sahl, S. J.; Hell, S. W.; Jakobs, S. *Nat. Rev. Mol. Cell Biol.* **2017**, *18*, 685-701.
(29) Albertazzi, L.; van der Zwaag, D.; Leenders, C. M. A.; Fitzner, R.; van der Hofstad, R. W.; Meijer, E. W. *Science* **2014**, *344*, 491-495.
(30) Berro, A. J.; Berglund, A. J.; Carmichael, P. T.; Kim, J. S.; Liddle, J. A. *ACS Nano* **2012**, *6*, 9496-9502.
(31) Onogi, S.; Shigemitsu, H.; Yoshii, T.; Tanida, T.; Ikeda, M.; Kubota, R.; Hamachi, I. *Nat. Chem.* **2016**, *8*, 743-752.
(32) Oracz, J.; Adolfsson, K.; Westphal, V.; Radzewicz, C.; Borgstrom, M. T.; Sahl, S. J.; Prinz, C. N.; Hell, S. W. *Nano Lett.* **2017**, *17*, 2652-2659.
(33) Stohr, R. J.; Kolesov, R.; Xia, K. W.; Reuter, R.; Meijer, J.; Logvenov, G.; Wrachtrup, J. *ACS Nano* **2012**, *6*, 9175-9181.
(34) Verzhbitskiy, I. A.; De Corato, M.; Ruini, A.; Molinari, E.; Narita, A.; Hu, Y.; Schwab, M. G.; Bruna, M.; Yoon, D.; Milana, S.; Feng, X.; Müllen, K.; Ferrari, A. C.; Casiraghi, C.; Prezzi, D. *Nano Lett.* **2016**, *16*, 3442-3447.
(35) Lieber, E.; Rao, C. N. R.; Chao, T. S.; Hoffman, C. W. W. *Anal. Chem.* **1957**, *29*, 916-918.
(36) Rust, M. J.; Bates, M.; Zhuang, X. W. *Nat. Methods* **2006**, *3*, 793-795.
(37) Dertinger, T.; Colyer, R.; Iyer, G.; Weiss, S.; Enderlein, J. *Proc. Natl. Acad. Sci. U. S. A.* **2009**, *106*, 22287-22292.
(38) Gustafsson, N.; Culley, S.; Ashdown, G.; Owen, D. M.; Pereira, P. M.; Henriques, R. *Nat. Comm.* **2016**, *7*, 12471.
(39) Zschieschang, U.; Klauk, H.; Mueller, I. B.; Strudwick, A. J.; Hintermann, T.; Schwab, M. G.; Narita, A.; Feng, X. L.; Muellen, K.; Weitz, R. T. *Adv. Elec. Mater.* **2015**, *1*, 1400010.

Table of Contents artwork